Effects of crack morphology on soil carbon flux dynamics in a dryland vertisol

Article *in* Geoderma · June 2020

DOI: 10.1016/j.geoderma.2020.114478

2 authors, including:

Keita Decarlo
Princeton University
5 PUBLICATIONS **53** CITATIONS

SEE PROFILE

Geoderma 375 (2020) 114478

Contents lists available at ScienceDirect

Geoderma

journal homepage: www.elsevier.com/locate/geoderma

Effects of crack morphology on soil carbon flux dynamics in a dryland vertisol

Keita F. DeCarlo[a,*], Kelly K. Caylor[b,c]

[a] Department of Civil & Environmental Engineering, Princeton University, Princeton, NJ 08544, USA
[b] Department of Geography, University of California, Santa Barbara, CA 93106, USA
[c] Bren School of Environmental Science & Management, University of California, Santa Barbara, CA 93106, USA

ARTICLE INFO

Keywords:
Bioturbation
Biocompaction
Soil cracks
Carbon flux
Thermal convection
Soil respiration

ABSTRACT

CO_2 flux in dryland ecosystems is typically limited by soil carbon release, resulting in pulses of flux with precipitation and transitions between low and high moisture. Soil crack morphology, which shifts distinctly between these wet and dry periods, can introduce additional complexity to the magnitude and dynamics of CO_2 flux, though its full effects remain unknown. In this study, we combine analyses of minute-scale temperature profile fluctuations in a model soil fracture with CO_2 flux measurements in Kenyan vertisols with known differences in crack morphology. We show that flux enhancements due to crack morphology are due to thermal convection and are driven by depth and aperture. Combined with elevated levels of carbon in the soil, fluxes can consistently increase several orders of magnitude. However, limitations imposed on either axis of soil mechanics or soil carbon release modulate the magnitude of CO_2 flux and increase variability. Our results provide a stronger integration of the role that soil structure plays on dryland CO_2 flux dynamics.

1. Introduction

Soil respiration is the largest and most variable terrestrial source of CO_2 flux to the atmosphere, with a net annual flux of 75–77 Pg C/ yr (Raich and Potter, 1995; Schlesinger and Andrews, 2000) and an estimated increase of 3.3 Pg/yr (Follett, 2001). Terrestrial carbon pools are estimated at 1550 and 750–950 Pg C for soil organic/inorganic carbon (Batjes, 1996; Eswaran et al., 1993; Schlesinger, 1995); and 600 Pg C for terrestrial vegetation (Houghton, 1995; Schimel, 1995). Fluxes to and from these pools are highly sensitive to changes in climate (Cox et al., 2000; Raich et al., 2002) and understanding their governing mechanisms is crucial for delineating future changes to soil-atmosphere CO_2 flux.

However, the contribution to global atmospheric CO_2 by dryland soils, which cover 40% of the Earth's land surface (Reynolds et al., 2007), remains an open question due to its under-representation in the literature (e.g., Bond-Lamberty and Thomson, 2010). In many mesic ecosystems, soil respiration is typically modeled using exponential relationships between temperature, water content, and substrate supply (Davidson et al., 2006), showing co-varying relationships between precipitation and temperature in response to phenological changes (Davidson et al., 1998). However, in dryland soils, these individual parameters may have separate temporal relationships (Reichstein et al., 2002; Tang and Baldocchi, 2005). In particular, carbon respiration exhibits a pulsed nature in response to changes in precipitation and soil moisture, being tightly coupled to seasonal distribution of rainfall but also magnitude of individual rainfall events (Loik et al., 2004). For example, re-wetting-induced fluxes can be up to 5 times greater than those from soils that were continually wetted (Fierer and Schimel, 2003; Huxman et al., 2004), often characterized as the Birch effect (Birch, 1958). These pulses contribute to a significant portion of the total CO_2 efflux from dryland soils (Liu et al., 2002; Thomas et al., 2008; Xu et al., 2004). This pulse is high but often short-lived, returning back to pre-hydrated levels within days (Thomas and Hoon, 2010). Several biotic factors have been theorized, including soil organic matter exposure following the break-up of aggregates (Appel, 1998; Denef et al., 2001) and the use of soil microorganisms that died during desiccation as substrate for the newly forming soil microfauna (Luo and Zhou, 2006).

Abiotic factors can also make a large contribution to soil-atmosphere CO_2 flux, particularly in the form of changes to gas transfer mechanisms. Diffusion occurs across all permeable interfaces (Allaire et al., 2008) and is often considered the dominant or only process for gas transport in low-permeability porous media (Moldrup et al., 2004).

Abbreviations: BT, Bioturbation; BC, Biocompaction; C, Control

* Corresponding author at: Department of Civil & Environmental Engineering, 59 Olden Street, Princeton University, Princeton, NJ 08544, USA.
E-mail address: kdecarlo@princeton.edu (K.F. DeCarlo).

https://doi.org/10.1016/j.geoderma.2020.114478
Received 21 November 2019; Received in revised form 9 May 2020; Accepted 24 May 2020
0016-7061/ Published by Elsevier B.V.

However, advective processes can play a larger role under higher permeability ranges (You and Zhan, 2013) and can even dominate fluxes (Massman et al., 1997; Weisbrod and Dragila, 2006). Specific examples of advective gas transfer include barometric pumping (Weeks, 1993; Weisbrod and Dragila, 2006), surface winds (Lewicki et al., 2003; 2007), and thermal convection (Nachshon et al., 2008; Weisbrod et al., 2009). The consequences of these processes to CO_2 flux can be significant, as they often do not follow simple temperature/soil moisture relationships, display erratic and more variable flux distributions, and have fluxes several orders of magnitude higher than those typically observed with diffusion-dominated flux (e.g., Etiope, 1999; Sanchez-Canete et al., 2011). Contributions to net flux can be variable: at times, these advective fluxes can directly vent into the atmosphere (Weisbrod et al., 2009), and at others they can occur entirely within the subsurface, only increasing concentration gradients and elevating diffusive fluxes (Levintal et al., 2017). These complex dynamics are due to the close relationship between flux and macropore morphology, often in the form of faults or fracture (Kuang et al., 2013). However, field studies have often focused on particular geological cases like those in rock faults (Weisbrod et al., 2009) or karst systems/subterranean caves (Sanchez-Canete et al., 2011; Breecker et al., 2013). Often reliant on steep temperature gradients and regular shifts in moisture content or porosity, these gas transfer processes likely play a significant role in the alteration of flux in dryland soils (Kowalski et al., 2008; Serrano-Ortiz et al., 2010), but few studies have quantified their relative importance or temporal and spatial variation (Rey, 2015).

These processes may be particularly present and dominant in shrink-swell soils. Also known as vertisols, they have an extensive presence across the globe (Ahmad and Mermut, 1996), but are also primarily located in water-limited tropical and sub-tropical zones, with 80% of vertisols in Australia, India, and East Africa (Virmani et al., 1982). Their high montmorillonite and smectite clay fraction results in high soil fertility and productivity (e.g., Ikitoo et al., 2011), but they can also develop deep soil cracks under drying conditions which persist throughout the soil profile through multiple wetting/drying events (Miller et al., 2010; Stewart et al., 2015). These soil cracks display the permeability properties necessary for significant advective gas transfer (e.g., Kishne et al., 2009; Miller et al., 2010) and exhibit anomalous and variable subsoil CO_2 concentrations associated with subsidence behavior and thus crack development (Breecker et al., 2013). Crack morphology and connectivity in the upper soil layer (0–0.25 m), where most biogenic sources of carbon are located, have been shown to exhibit large variability despite similar soil moisture ranges due to biophysical effects (DeCarlo and Caylor, 2019), but to our knowledge, studies on cracked dryland soils that combine in-situ morphological properties and CO_2 flux dynamics have not been published.

We outline a theoretical conceptualization of how these two elements may be linked, using DeCarlo and Caylor (2019) as a reference (Fig. 1). Two major controls associated with these biologically active vertisols are first defined: 1.) soil crack mechanics, and 2.) soil carbon release. In the control (C) soils, where carbon release is relatively low and cracking is minimal, fluxes are dominated by standard diffusion processes (Fig. 1A). In the biocompacted (BC) soils, where the soil is biologically similar but deep cracks are present due to faunal activity on the surface, carbon release is also relatively low, but fluxes are mechanically enhanced due to thermal gradients present during the nighttime hours (Fig. 1B). In the bioturbated (BT) soils, where termites are active, carbon release is relatively high, but fluxes are mechanically limited due to the insufficient depth of the otherwise wide cracks formed (Fig. 1C). Finally, in the deep termite burrows of the BT soils, carbon release is high and are dominated by convective flows (Fig. 1D). Fig. 1F shows how these four permutations may results in different carbon flux signatures, given otherwise uniform conditions in terms of water content, microbial content, etc. Distributions here are shown in the form of inverse cumulative probability distributions. In mechanically-limited/carbon-limited cracked soil systems (C), we expect diffusive fluxes to result in a fairly uniform distribution; assuming consistent termite activity, the introduction of higher carbon release (BT) would result in a higher-magnitude distribution that otherwise retains the diffusion flux signature. Shifting to carbon-limited but mechanically-enhanced (BC) soil systems, we would expect periodically large fluxes as a result of the venting process interspersed between lower diffusive fluxes, resulting in a wide distribution of flux. A similar signature, albeit with a higher magnitude and range due to high carbon release, would be expected in the carbon-enhanced variant (BT burrows). The objective of this present study is to experimentally elucidate these links between diurnal-scale CO_2 flux and different crack morphologies and connectivity, using the same soil systems and conditions. This would allow us to provide a more mechanistic and physically-based understanding of the complex CO_2 dynamics observed in dryland soils.

2. Materials and methods

2.1. Crack field site selection

Our soils were located on vertisols located in the Mpala Farm in Laikipia District, central Kenya. They are part of a semi-arid savannah ecosystem with mean annual precipitation of 600 mm/year, though annual variability is high, ranging between 350 and 1000 mm/year observed in the past two decades. Peak rainfall is usually in April and November, with dry seasons in the summer and early winter. On 13 of the 19 days between June 17th to July 5th, an uncharacteristic series of small to moderate rainfall events took place, totaling 76 mm. Prior to this, the field site had not seen a major or minor rainfall event since May 13th (25.7 mm) and May 24th (1 mm), respectively. Afterwards, rainfall effectively ceased until the tail end of experiments. As such, we used this well-timed event to characterize the effect of a naturally-induced precipitation and soil moisture pulse on crack-induced CO_2 flux. We classify the data collected prior to June 17th, between June 17th and July 5th, and July 5th onwards as pre-wetting, wetting, and drying data, respectively. We show the temporal distribution and magnitude of all precipitation events during the course of experiments in Table 1.

The vertisols in our field sites have a large native biodiversity presence, including over 40 large mammal species, and an extensive termite habitation. This variable faunal activity is capable of inducing divergent crack morphologies in the vertisol despite otherwise comparable soil physicochemical properties, including soil moisture and cation content. The faunal biophysical activity (or lack thereof) and the resultant crack morphology are as shown below (please refer to DeCarlo and Caylor, 2019 for details on the quantitative differences in crack morphology between the soil types, as well as the full statistics of the physicochemical properties of the soils in our field sites):

I. Reference soil (C): these are termite-free soils dominated by patchy vegetation inside the Kenya Long-Term Exclusion Experiment (KLEE) plots (Young et al., 1997), which use electric fences to exclude all large herbivores from a 200 m × 200 m space. Relative to the other soil types investigated, crack porosity and maximal depth are minimal.
II. Biocompacted soil (BC): these are the long, narrow animal trails regularly used by various megaherbivores in the region over multiple years. Cracking in these soils are deep, with a moderate crack porosity and large maximal depth.
III. Bioturbated (BT) soil: these are the lenticular soil mounds formed by fungus-cultivating termites (Macrotermitinae, Odontermes), which range anywhere between < 1–10 m, and which are regularly distributed at a spacing of 50–100 m (Bonachela et al., 2015). Maximal crack depth is low, but crack porosity is highest of the three soil types. Within the BT soils, termites also manually dig several deep, stable burrows used for entry and exit of their nests.

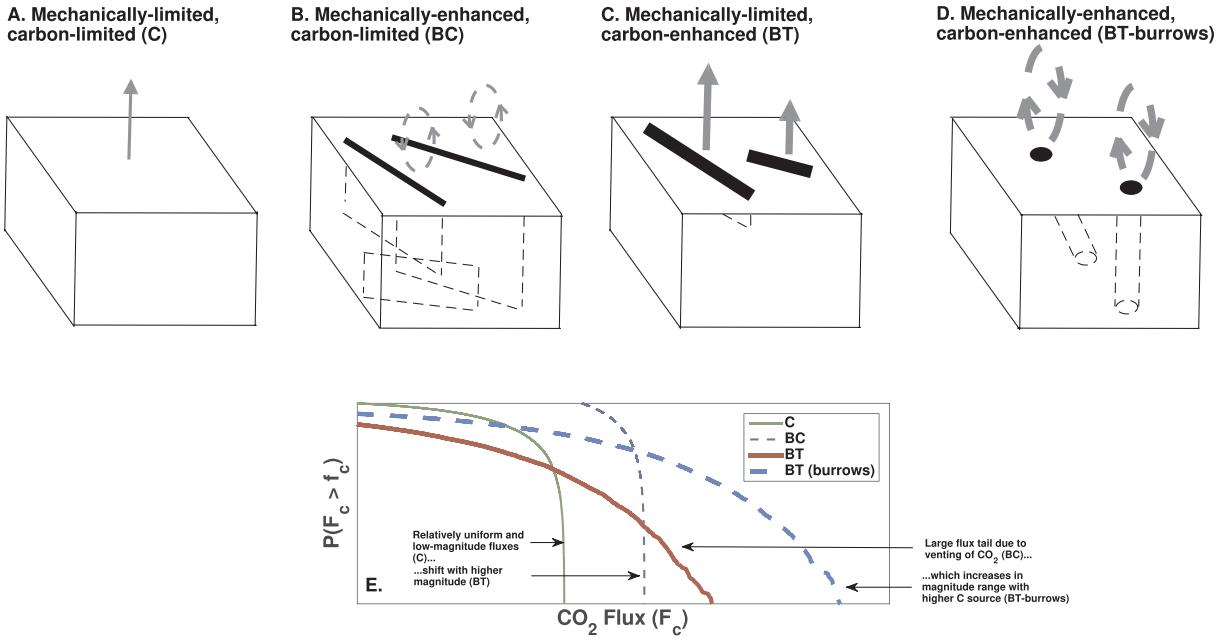

Fig. 1. Conceptual outline for the link between crack morphology and carbon flux in faunally active vertisols: (a-d) visual schematic flux processes in the four soil classifications outlined in DeCarlo and Caylor (2019), and (f) their theoretical inverse cumulative distributions, plotted in log–log space.

Table 1
List of all precipitation events by date and magnitude during the course of experiments.

	Date	Precipitation [mm/day]
Wetting Phase	17-Jun	1.815
	18-Jun	7.031
	19-Jun	2.265
	20-Jun	4.538
	22-Jun	7.247
	23-Jun	6.124
	24-Jun	0.452
	25-Jun	14.173
	29-Jun	3.174
	1-Jul	3.629
	3-Jul	5.784
	4-Jul	14.741
	5-Jul	5.103
Drying Phase	12-Jul	0.452
	28-Jul	3.517
	29-Jul	2.381
	30-Jul	1.701
	31-Jul	4.534

Within this classification, we chose 4 sites in the C soil and 6 sites in the BT soils, located in 3 of the 4 termite mounds used in DeCarlo and Caylor (2019), including 3 sites of BT burrows (defined explicitly as the distinct round holes dug by the termites to connect their nest to the overlying atmosphere), located in the largest termite mound. Given the regular megafaunal presence and the mechanical consequences on intact crack morphology, our BC soil sites were more variable, and consequently more numerous. We measured a total of 17 sites, of which 5 commenced from the beginning of the season, 2 commenced 2 weeks after start, and the last 10 commenced after the end of the rain events, 1 month after start. Of these, 2 sites were trampled by megafauna during the season and were rendered unusable. Volumetric soil moisture content is measured using a Hydrosense probe (CD/CS620, Campbell Scientific), immediately adjacent to the flux measurement, where the probe was inserted in the topmost layer of the soil (< 5 cm). Due to equipment problems, we could not start making soil moisture measurements until the middle of the wetting phase of our experiments.

2.2. Fracture temperature profile

We dug a square hole measuring 15 × 15 × 20 cm in sandy non-vertic soil immediately adjacent to our field station in order to create a static soil "frame" for our model fracture. All soil boundaries were covered with sealed plastic tarp except the top surface, and we packed the hole with BC soil gathered from our field sites to create a stable model fracture measuring 2.5 × 5 × 20 cm (width × length × depth). The soil was collected dry, and then wetted to help create the appropriate shape, and left to dry and set for 5 days. Note that as this soil was excavated, reconsolidated, and manually packed into the hole, it retains virtually none of the fauna-influenced structural properties characterized prior in the BC soils. We then coiled 5 thermocouples (Type T SLE – 0.81 mm diameter, Omega) each on 4 metal rods, with 5 cm spacing between each, and placed them 5 cm apart within the fracture, thereby creating a grid of temperature measurements at 5 cm increments in all directions. We record temperature using a datalogger (CR1000X, Campbell Scientific) and thermocouple multiplexer (AM25T, Campbell Scientific) every minute for 24 h starting at 8 h30 on August 11th, 2015. Given that the morphology of the model fractures is in a similar order of magnitude as the ones observed in the field and that the same soil types were used, we assume that temperature profile of the model fracture is comparable to that of the fractures in the field sites.

We analyze the temperature profile of the model fracture in order to observe mechanical enhancements (i.e., thermal convection) on air fluxes within a fracture. Specifically, we use the Rayleigh number, which is a dimensionless number that compares buoyancy and viscosity, to evaluate the potential for fractures to induce free convection:

$$Ra = \frac{\Delta T \alpha g k L}{\nu \kappa} \quad (1)$$

where ΔT (°C) is the temperature difference between fracture air across length scale L (m), α = 0.00367 (1/°C) is the thermal expansion coefficient, g is the gravitational constant (m/s^2), k is the fracture permeability (m^2) (k = (2b) ^{2}/12, where 2b is the fracture aperture), ν = 1.5 × 10^{-5} (m^2/s) is the kinematic viscosity, and κ = 2 × 10^{-5} (m^2/s) is the thermal diffusivity. Free convection in fracture will theoretically occur when Ra exceeds a critical value of 4π^2 (Lapwood, 1948; Nield, 1982), roughly equal to 40, and is linearly correlated with

the temperature gradient and quadratically related to fracture permeability.

2.3. CO_2 flux measurements

Our CO_2 flux measurements were made between June 13th and July 29th, 2016 – thus measurements were made in the midst of the dry season. A steady-state, dynamic closed chamber system (14.7 cm height, 15 cm internal diameter) attached to an infrared gas analyzer (IRGA; LI-840, Li-Cor, Lincoln, NE, USA) and a miniature diaphragm pump (1.0 L/min flow rate; 3014 series, Denver-Gardner, Milwaukee, WI, USA) was used for CO_2 efflux measurement (see Rochette et al., 1997 for an example of a dynamic closed chamber soil respiration setup). We made manual measurements 5 times a day, at 6 *h*00, 12 *h*00, 18 *h*00, 22 *h*00, and 2 *h*00 the following day – a minority of time points are missing due to the logistical difficulty of making the number of measurements made every 4–6 h. Measurements were taken by setting the chamber on the soil site for 2–4 min and recording measurements at 5 s intervals. Soil efflux rate was calculated using a least-squares fit on the rate of CO_2 concentration increase in the chamber for at least the last minute of data, corrected for mean experimental temperature and pressure, and the volume of the chamber. We only used measurements that showed a consistent linear trend in CO_2 accumulation within the chamber – a small minority of data where concentration rate was erratic was discarded.

We did not place soil collars into our soil sites. We justify this action given the unique experimental considerations of our study and vertisol properties, and how the known consequences will likely outweigh the potential benefits of collar insertion. Firstly, given how hard the soil becomes, it is logistically impossible to place soil collars into dry vertisols without destroying the crack structure we seek to study. Carefully excavating the soil to place collars is not an option either given the large soil peds formed by the dried vertisol – attempts to manually make smooth cuts into the soil requires breaking the aggregates, which will not only greatly disturb the soil structure, but also create large artificial "fractures" along both the inside and outside of the collar, due to the uneven fit of the collar. Inserting the collars when wet, while facilitating placement of the collars, is also not an option, as this would destroy the very crack structures we seek to study, and furthermore, would still create the aforementioned artificial "fractures" along the collar. As such, we opted to firmly but carefully push our chambers on top of our field sites and cover the surrounding 1 m of the soil in all directions with a tarp sealed around the chamber, to minimize air entry and exit between the chamber and the atmosphere. Furthermore, we filled the crack present in the vicinity of the measurement sides on all sides outside of the chamber with vertic soil for approximately 10–20 cm to further minimize air leakage and entry.

3. Results

3.1. Fracture air thermal dynamics

Temperature values of fracture air measured in the model crack are shown by depth for the two central horizontal length positions, at x = 5 (Fig. 2A) and 10 cm (Fig. 2B) – equipment failure for the 0 and 15 cm lengths precluded their data usage. Like other typical soil temperature profiles, we observe high amplitude at the surface (x = 0 cm), with larger daytime variability and smaller nighttime variability. Likewise, we observe low amplitudes and variability at 20 cm depth for both horizontal lengths. Two sharp drops in surface temperature were observed at 12 h and 15 h, possibly due to cloud cover (no rain was observed on this day). A large upward spike of 12 °C occurred at 12 h46 at 5 cm length and 10 cm depth for 3 min, being brought up to surface air temperature, after which it returned to its pre-spike value. As we did not observe it at any other depth and was for a few minutes, we assumed it to be due to falling surface debris. However, several distinct phenomena were observed in our profile, mostly in the nighttime hours. The temperature profile at 5 cm depth and 5 cm length showed regular downward dips in temperature by 2–5 °C, roughly between the hours of 18 h and 8 h. These events often lasted for a single time point (1 min) and brought them to a temperature 1–2 °C of that of the surface. We also observed regular upward spikes in temperature at 5 cm and 10 cm length during the same hours, though the magnitude was lower, at around 1.5–2 °C. Finally, the temperature profile at 10 and 15 cm were virtually identical at the nighttime hours for both 5 and 10 cm length, only decoupling in the daytime.

We calculated maximum Ra observed at each soil depth as a function of crack aperture and compare them with crack aperture distribution of the BC soil sites analyzed in DeCarlo and Caylor (2019) in Fig. 3 – we assumed that a similar temperature profile is present in both the model fracture and the BC soil sites. Mean crack aperture was 0.27 cm, with 14% of crack apertures at 0.3 cm and above, distributed as a long tail. Meanwhile, maximum Ra first exceeds that of the critical value at a crack aperture of 0.28 cm, between 5 and 10 cm depth, which corresponds to a fracture permeability of 6.53×10^{-7} m^2 – the minimum crack aperture above which Ra first exceeds the critical value at all depths is approximately 0.6 cm.

Acute dips observed in the temperature profile of our model soil fracture at 5 cm depth, observed only at night, are likely to be individual cold air intrusions from surface air at localized points, as we only see them at the 10 cm length. To further quantify this, we correlated minute-scale temperature fluctuations between spatially adjacent soil subsections using the Pearson correlation coefficient – spatially adjacent locations that both show simultaneous increases or decreases in temperature will have a positive value, while those that show opposing responses will have a negative value. The closer to −1 or 1, the stronger the correlation. Two strong correlations between fluctuations are shown in Fig. 8A (positive correlation, between 5 and 10 cm length at depth of 0 cm at daytime) and 9B (negative correlation, between 5 and 10 cm length at depth of 5 cm at nighttime). We plot the correlation between each spatial location with a line in Fig. 8C and D for the day and night, where color indicates a positive or negative correlation – only strong correlations, which we arbitrarily set at an absolute value above 0.5, are shown. Daytime correlations showed that increases or decreases in temperature were positively correlated throughout the soil profile, likely due to natural gradual changes observed throughout the course of the day. At night, we observed a shift in the upper half of the soil: at 10 cm length, between 0 and 5 cm depth (hereby labeled as location 1 and 2), a strong positive correlation was observed, which means that the individual dips in temperature observed in the soil profile at location 2 corresponded with dips observed only at the surface immediately above it. Note that no correlation is observed between location 2 and the other surface temperature site, which means that this effect was localized. Simultaneously, at the same depth, but at 5 cm length (hereby labeled as location 3), we observed a corresponding increase in temperature, quantified by the strong negative correlation between the two locations. Note that as location 2 was positively correlated with location 1, location 3 was also negatively correlated with location 1 as well. This result suggests that cold air intrusion, initiating at location 1, penetrated the fracture to a depth between 5 and 10 cm, which then displaced the warmer air below location 2 laterally and upwards, resulting in warmer air at location 3 and thus higher temperature. Given the strong correlation and our timescale, this process occurred within a minute-timescale. We plot convection cell magnitude and temporal distribution in Fig. 9. We defined the onset and cessation of a convection cell as when the temperature at 5 cm depth decreased and increased over 0.5 °C/min, respectively (i.e., each downward spike in the dark red line in Fig. 2A). A total of 121 individual convection cell events was observed, of which all lasted 3 min or less (N_{1min} = 113, N_{2min} = 6, N_{3min} = 2). The distribution of temporal spacing between convection cell events and the frequency of intrusion magnitude were exponential in nature, with a mean event spacing of 5.09 min and a

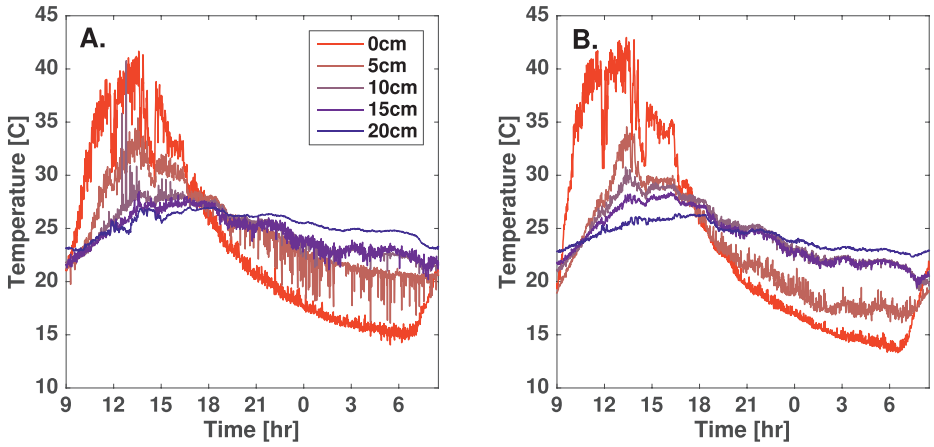

Fig. 2. Soil temperature profile of a model soil fracture with dimensions of 2.5 × 15 × 20 cm width, length, and depth, respectively, measured at (a) 5 cm length and (b) 10 cm length position. Temperature at depth was measured in 5 cm increments.

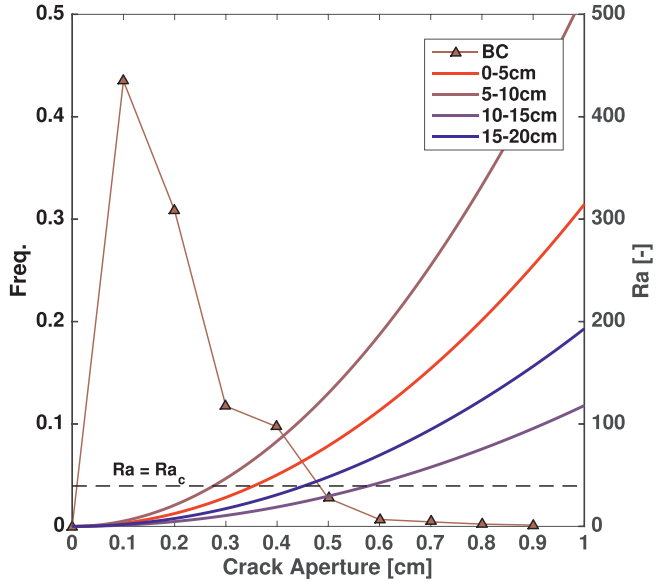

Fig. 3. Mean frequency and maximal Rayleigh number observed at each crack aperture. Mean crack aperture distributions represent the BC soil crack systems collected in DeCarlo and Caylor (2019) at 24.4% mean volumetric soil moisture. Temperature profiles obtained from the model soil fracture are used for Rayleigh number calculation.

mean intrusion value of 1.37 °C/min.

3.2. Wetting effects on CO_2 flux

Fig. 4A-B shows the CO_2 flux dynamics in the C and BC soils, respectively. Pre-wetting phase fluxes were comparable. The C soils in the wetting phase showed an increased mean flux, which remained elevated through the rest of the wetting phase, with no decreases in mean flux observed; a steady decline in mean flux was observed during the drying phase, despite minor upticks coinciding with later onset of rainfall at the end of the drying phase. Meanwhile, the BC soil flux in the wetting phase initially spiked by a factor of 5, after which flux decreased, though remaining at a flux rate higher than that of the C soil. BC soil CO_2 flux showed erratic behavior – flux early in the drying phase remained elevated and higher than the C soils, after which they decreased markedly below that of the C soils. The BC soil fluxes then spike once more, doubling those of the C soil fluxes in the middle/end of the drying phase.

Fig. 4C-D shows the CO_2 flux dynamics in the BT soils and its burrows, respectively, both of which are considerably more elevated than those in the C or BC soils. Pre-wetting phase fluxes vary by a factor of 4. Mean BT soil flux rates decreased during the drying phase, though not as consistently as those in the C and BC soils. The BT burrows, which still were part of active termite mounds, showed the largest fluxes overall, being almost two orders of magnitude higher than even the BT soils themselves. BT burrow fluxes decreased dramatically during the drying phase, but even then, they were comparable to the outlier BT soil fluxes near the end of the drying phase.

Mean flux rates did not reflect the change in CO_2 flux distribution observed in many of the soil types, which explained some of the variability observed in our results. The C and BC soils showed comparable flux distributions in the pre-wetting phase. The range of C soil fluxes in the wetting phase increased, with outlier C soil fluxes higher than the mean flux by a factor of 2. This was considerably more pronounced in the BC soils in the wetting phase – in addition to the increased variability, outlier fluxes were up to an order of magnitude higher than the mean CO_2 flux, which itself was double that of the C soil. In the drying phase, overall magnitudes of the C soil fluxes decreased despite flux variability being higher than in the pre-wetting phase. Meanwhile, outlier BC soil fluxes higher than the mean flux by a factor between 4 and 20 persisted throughout the drying phase.

3.3. Diurnal effects on CO_2 flux

Diurnal CO_2 variability in the C and BC soils, and the BT soils and their burrows within the three moisture regimes is plotted in Figs. 5 and 6. Measurements from the pre-wetting phase in the BT burrow soils, and from 2 h in the wetting phase in the C and BT soils are missing due to either logistical or equipment issues.

In the pre-wetting phase in the C soils, we observed little variability between hour of day measured, though measurements taken at 6 h were slightly lower. In the wetting phase, mean flux values were highest at 12 h, with its range almost double that of those at the other time points. This trend diminished slightly in the drying phase, though the highest outlier fluxes were observed at 12 h. In the BC soils, we observe that mean flux and distribution were comparable to those in the C soils at all hours of the day save for those at 2 h, whose flux values were higher than the others by a factor of 3. In the wetting phase, this trend was reversed – fluxes were roughly 3 times higher at 12 h compared to the other time points, with the highest outlier flux value observed at this time point. In the drying phase, this trend diminished, with outlier flux values observed at all time points, though the highest values were still observed at 12 h.

BT soils did not show significant diurnal effects: during the pre-wetting and drying phase, outlier flux values were spread across time

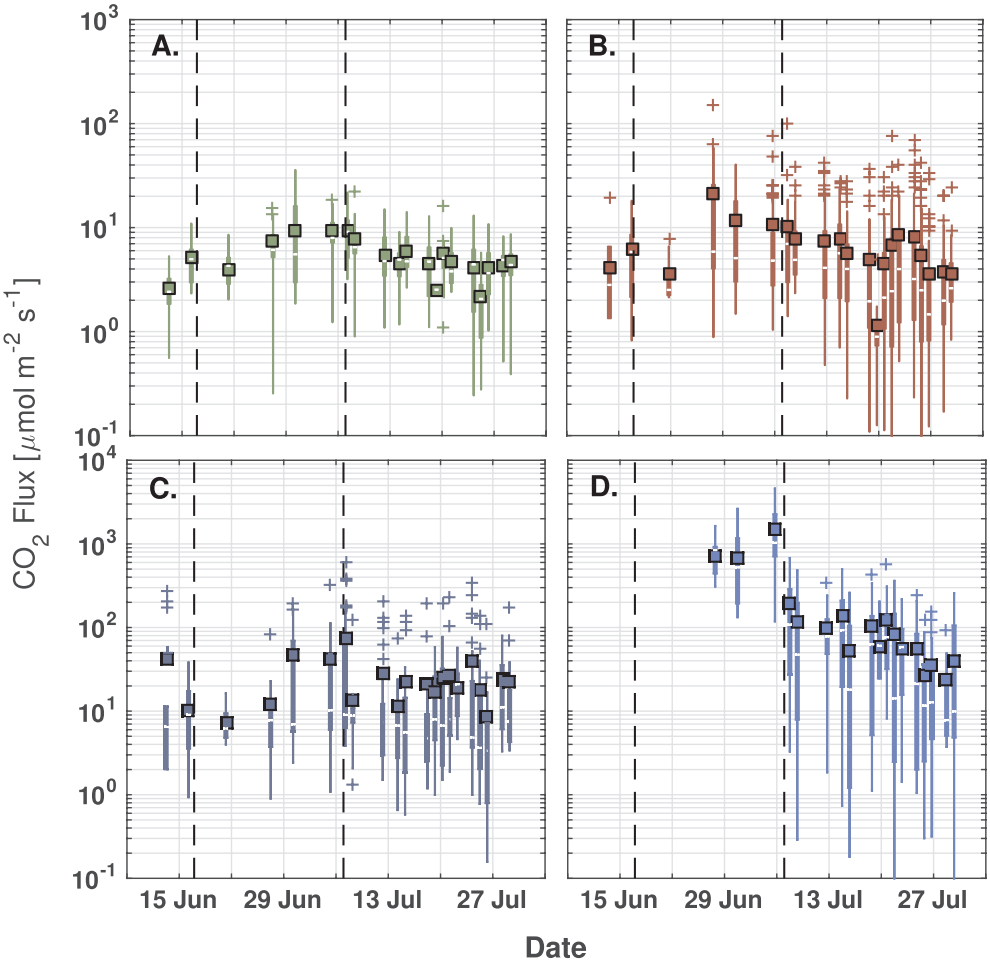

Fig. 4. CO_2 flux distribution of the (a) C, (b) BC, (c) BT, and (d) BT burrow soils over the length of experiments. Dotted lines indicate the boundaries between the pre-wetting, wetting, and drying phases. For each box plot, mean is shown by the square box with black edge, median by the white dash, the 25th and 75th quartile by the box (i.e., the thick central line), and the highest/lowest datum within 1.5 times the inter-quartile range by the whiskers (i.e., the thinner outer lines). All outliers are plotted with a + sign. Each box plot includes all measurements made for that day. 1Note the axis difference between the C and BC soils, and BT and BT burrow soils.

points; during the wetting phase, outlier fluxes were present at 6 h and 12 h. In the burrow soils, during the wetting phase, flux values seemed to show significant divergence at 22 h, where mean flux was approximately 3 times larger than at other time points, and with virtually no variability (n = 2). Distribution magnitude decreased in the drying phase to a level comparable to that of the drying phase in the BT soils, and outlier fluxes were similar as well.

3.4. Soil moisture effects on CO_2 flux

CO_2 flux variability in the soil types by soil moisture range is plotted in Fig. 7. Note that this only compares fluxes from the second half of the wetting phase and the drying phase – no pre-wetting phase values are included here. Mean flux values and distribution remained relatively constant between the soil moisture range of 0.2 and higher – flux values progressively decreased at soil moisture ranges of 0.1–0.2, and < 0.1. In the BC soils, flux variability seemed to increase with progressively lower soil moisture below 0.2–0.3, with the lower quartiles of CO_2 flux steadily decreasing. A large number of outlier fluxes were observed at soil moisture ranges of 0.1–0.2, and 0.5–0.6. BT soils showed flux variability ranging between several orders of magnitude across all soil moisture ranges, and mean flux shows an exponentially increasing trend with higher soil moisture. A large number of outlier fluxes were observed at a soil moisture range of 0.1–0.2. BT burrow soils show a similar trend overall as well, albeit with higher values.

4. Discussion

Despite originating from the same vertisol in a single dryland environment within a single drying season, with individual sites all within 2–3 km of one another, mean CO_2 efflux ranged from a minimum of 1.13 μmol m^{-2} s^{-1}, observed in the BC soils 2 weeks into the drying phase, to a maximum of 1465.3 μmol m^{-2} s^{-1}, observed in the BT burrows at the end of the wetting phase. Minimum mean CO_2 efflux rate is on the lower end of mean soil efflux rates in water-limited environments compiled in Thomas et al. (2011), while maximum mean efflux rate is 4 times greater than its largest spike, which was measured after a wetting event of velvet mesquite (Sponseller, 2007). It is evident that a multitude of soil physical and biological processes govern the complex CO_2 dynamics observed in our field site. Here, we use the conceptual framework outlined in the beginning of this study (Fig. 1) outlining the two major relevant controls: crack mechanics, which is abiotic in nature; and soil carbon release, which is biotic in nature. Both operate on gradients that can either limit or enhance CO_2 flux. We outline the relevant environmental conditions that describe our CO_2 efflux results, and finally evaluate each permutation (mechanically-limited/carbon-limited, mechanically-enhanced/carbon-limited, mechanically-limited/carbon-enhanced, mechanically-enhanced/carbon-enhanced).

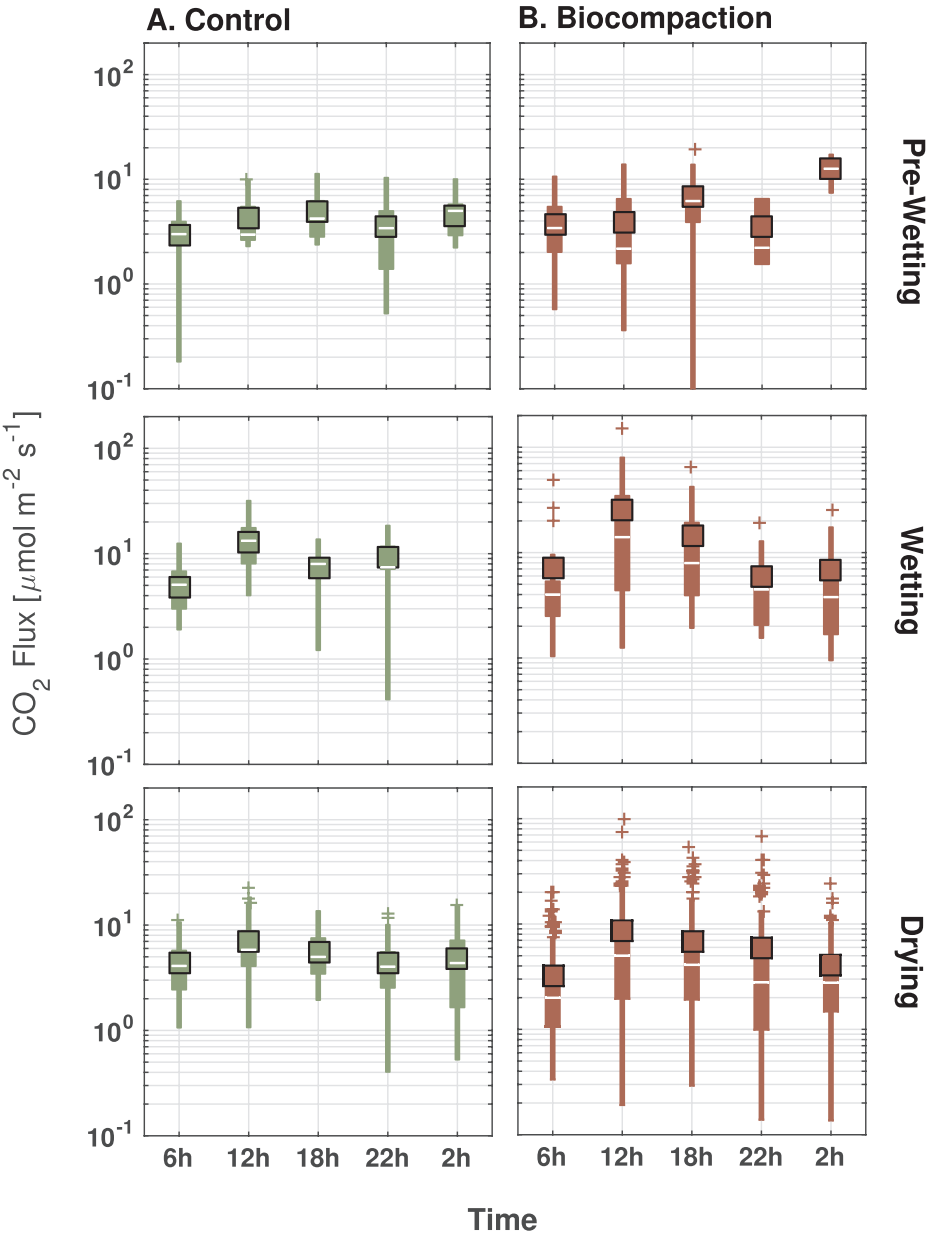

Fig. 5. CO_2 flux distribution of the (a) C and (b) BC soils by time of day in the pre-wetting, wetting, and drying phases.

4.1. Abiotic Factors: Soil structural mechanics

4.1.1. Thermal convection

Prior to discussing thermal convection, a brief discussion on the potential effects of surface wind (i.e., forced convection) is warranted. Research on constructed soil fractures have indicated 100% and 570% increases in evaporation at depths of 45 cm and 5 cm, respectively, when exposed to wind of 11.2 m s^{-1} (Adams and Hanks, 1964; Adams et al., 1969), with similar moisture loss values observed for crack widths of 0.65 cm and 1.91 cm (Selim and Kirkham, 1970). This effect cannot be entirely ruled out for the model fracture. However, given the extremely short duration of each convection event (93% of events were one minute or less), its exponential temporal spacing, and its exclusive occurrence in the nighttime hours (19 h-9 h) are all likely to be characteristics of thermal convection and not forced convection. Furthermore, the closed-chamber method of CO_2 flux measurements ensured that no surface wind effects are directly present on the soil surface measured, and both the tarp and soil burying precautions discussed in Section 2.4 have minimized surface wind effects. Thus, we assume that temperature profile and dynamics exhibited in our experiments display properties that reflect thermal convection.

Finger-flow patterns, whereby air is laterally displaced along the crack profile, are typical of fracture convection cells (Nachshon et al., 2008; Weisbrod et al., 2009), though our size and temporal dynamics vary. This is despite considerably steeper temperature gradients observed in our studies – surface measurements at night in our field studies dropped to around 15 °C at night, creating a fracture gradient of 10 °C over 20 cm, approximately 2–4 times larger than those characterized above. Thus, differences may be in part due to differences in crack morphology – Weisbrod et al. (2009) evaluated rock fractures that had a variable aperture of 1–5 cm, length of 2 m, and depth of $>$ 1 m, Nachshon et al. (2008) used Hele-Shaw cells with aperture of 1–2 cm, and 50 cm length and depth. Similarly, minimum fracture permeability for thermal convection onset is 4 times smaller in Levintal et al. (2017), which used artificial fractures with a depth of 1 m but lower temperature gradients than our model fracture, further enforcing this fact. The regular onset and arrest of convection cells in our model fracture may be due to transient disruptions in the soil air temperature

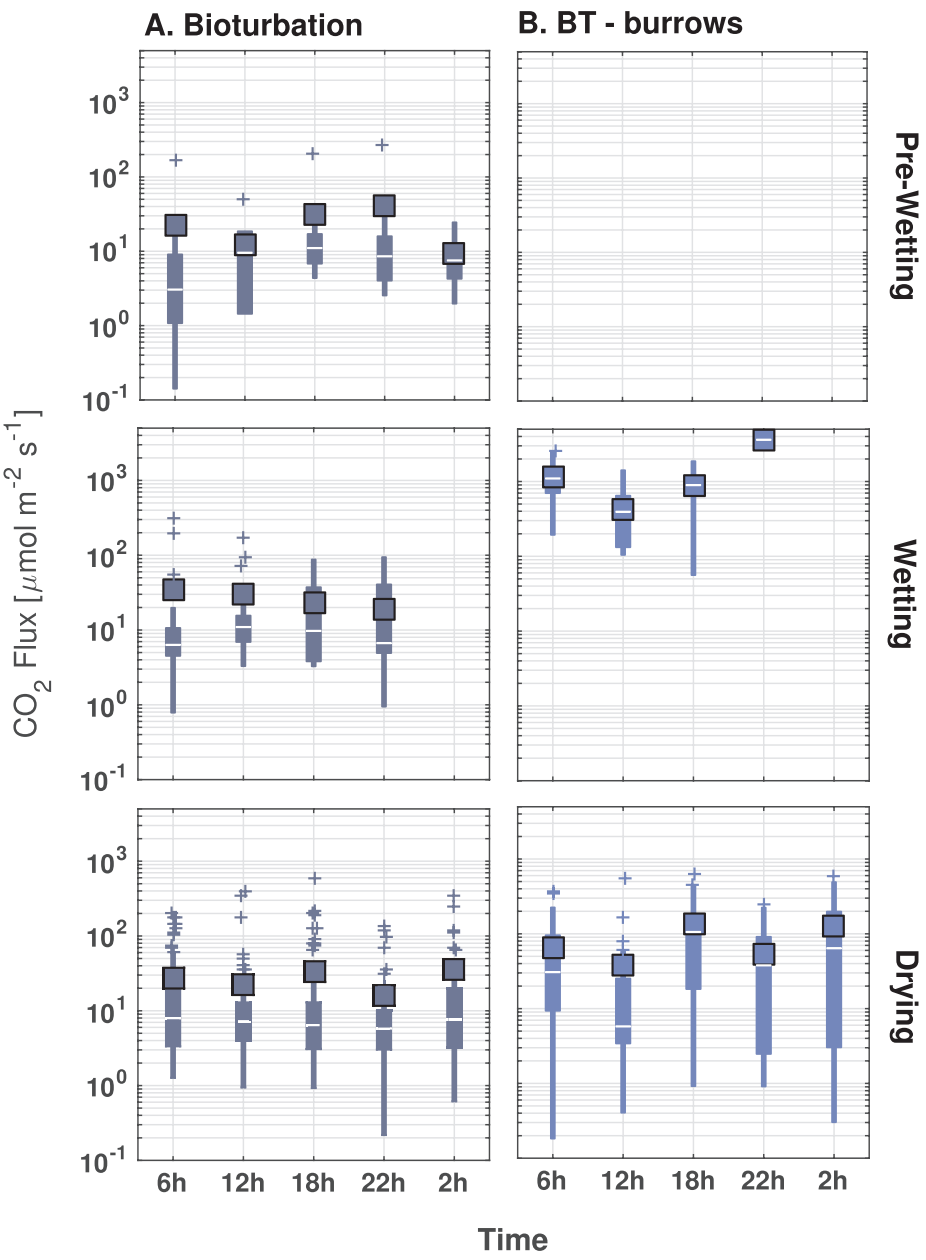

Fig. 6. CO_2 flux distribution of the (a) BT and (b) BT burrow soils by time of day in the pre-wetting, wetting, and drying phases. Note the axis difference between this and Fig. 5.

profile by the convection cells themselves, which serve as a natural negative feedback to the convection process – however, given the large surface area of the fracture, any cold air introduced in the soil is likely quickly warmed by the adjacent soil face, re-establishing the vertical temperature profile.

Larger fracture apertures showed a non-linear increase in maximum Ra, which suggests that the magnitude of convection observed in the fracture, and therefore that of air displacement and flux, at all soil profiles, will also increase non-linearly. This will likely result in exponentially higher fluxes from larger surface crack apertures. However, the consequences to overall air displacement and flux are offset by the exponential decrease of progressively larger crack apertures observed in a typical cracked soil surface. Therefore, assuming a uniform distribution and immediate release of a given gas in fracture, we can expect to see a highly non-linear distribution of that gas flux for soil sites affected by thermal convection, in the form of a multitude of small, non-convection influenced fluxes, and a small number of large, convection-influenced fluxes. Combined with the fact that convection cells may not necessarily reach the surface and be confined within the soil subsurface (Levintal et al., 2017), which still nevertheless enhance gas flux by reducing the diffusion length, we would expect to see a large spread in fracture-induced gas flux.

In addition to the deep soil fractures that characterize BC soils, BT burrows are likely to generate thermally-induced convection cells, which have the function of venting their natural habitats. Though the physical process is identical, wherein cold dense air displaces underlying the less dense hot air, the environmental conditions under which they form are slightly different – we expand further on this in Section 4.2.3.

4.1.2. *Vertisol morphology*

Despite similar mean CO_2 flux observed during the pre-wetting and drying phase, a number of outlier fluxes ranging between 20 and 100 μmol m^{-2} s^{-1} are observed in the BC soils, only during the drying

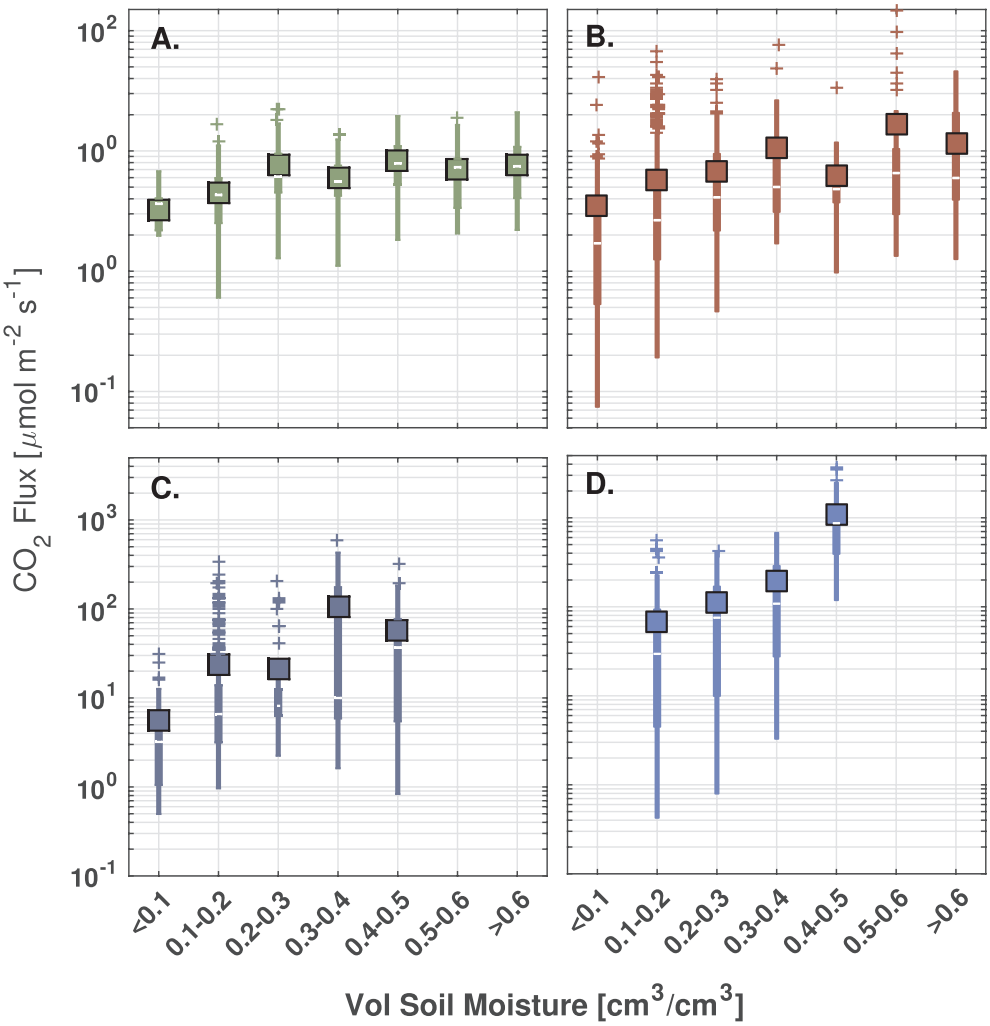

Fig. 7. CO_2 flux distribution of the (a) C, (b) BC, (c) BT, and (d) BT burrow soils by volumetric soil moisture. Note that these do not include fluxes from the pre-wetting, and the first half of the wetting phase due to lack of volumetric soil moisture measurements at this time. Also note axes differences between the C and BC soils, and BT and BT burrow soils.

phase. This may be due to particularities in vertisol crack morphology. Breecker et al. (2013) observed a steep, step-like decline in subsoil CO_2 concentration, from 10% to 0.1%, with steady declines in soil moisture. This was hypothesized to be due to the formation of soil cracks, which increase vertisol porosity and decrease tortuosity. This increases the coefficient of variation in subsoil CO_2 concentrations to almost double that of non-vertic soils (Flechard et al., 2007; Breecker et al., 2013), and likely contributes to the characteristic flux distribution spanning several orders of magnitude observed in other faulted/fractured soil systems (e.g., Etiope, 1999). In addition, a soil crack layering effect has been observed in our BC soils, where surface disturbance and swelling events seal only the upper sections of the crack and leave a crack void space at relatively shallow depth of 0–0.5 m (DeCarlo and Caylor, 2019). As new cracks form on a drying surface, a series of sustained outlier flux events would occur as the advancing cracks progressively open and expose deeper and deeper void spaces. This may also explain why pre-wetting phase flux shows lower variability and virtually no outlier fluxes, as maximum shrinkage of the soil has been reached, and all easily accessible air pockets were exposed.

4.2. Biotic Factors: Soil carbon release

The primary controls of soil respiration at the diel timescale are typically considered to be moisture pulse, temperature, and photosynthesis rate (Craine et al., 1999; Hogberg et al., 2001; Huxman et al., 2004; Xu et al., 2004; Tang et al., 2005; Baldocchi et al., 2006). We assume photosynthesis rate and autotrophic activity to be negligible given the timing of the dry season and that virtually all annual grasses had died by this stage, and we also note that moisture pulse and temperature are physical processes that also have abiotic consequences, as highlighted elsewhere in this paper. However, we focus here on its biotic influences and consequences of soil carbon supply, release, and utilization by heterotrophic communities.

4.2.1. Moisture pulse

Soil CO_2 efflux in the C and BC soils show a positive response to precipitation events, though the magnitude between the two vary. Thomas and Hoon (2010) artificially applied water to dry crusted soils – simulation of light rainfall (1.4 mm) resulted in a saturation depth of 0.004 m, which increased daytime fluxes from 2.6 μmol m^{-2} s^{-1} to a peak of 11.5 μmol m^{-2} s^{-1}, a 4 factor increase, while heavy rainfall (120 mm) resulted in a saturation depth of 0.31 m and an increase in daytime fluxes to 59.3 μmol m^{-2} s^{-1}, a 23 factor increase, and rainfall events of over 20 mm was characterized to be of sufficient size necessary to wet subsoil and result in sustained increases in CO_2 concentration beyond that of just superficial increases in flux. The largest rainfall events were 14.1 and 14.7 mm/hr, which are about an order of magnitude lower than the heavy rainfall simulation. However, soil

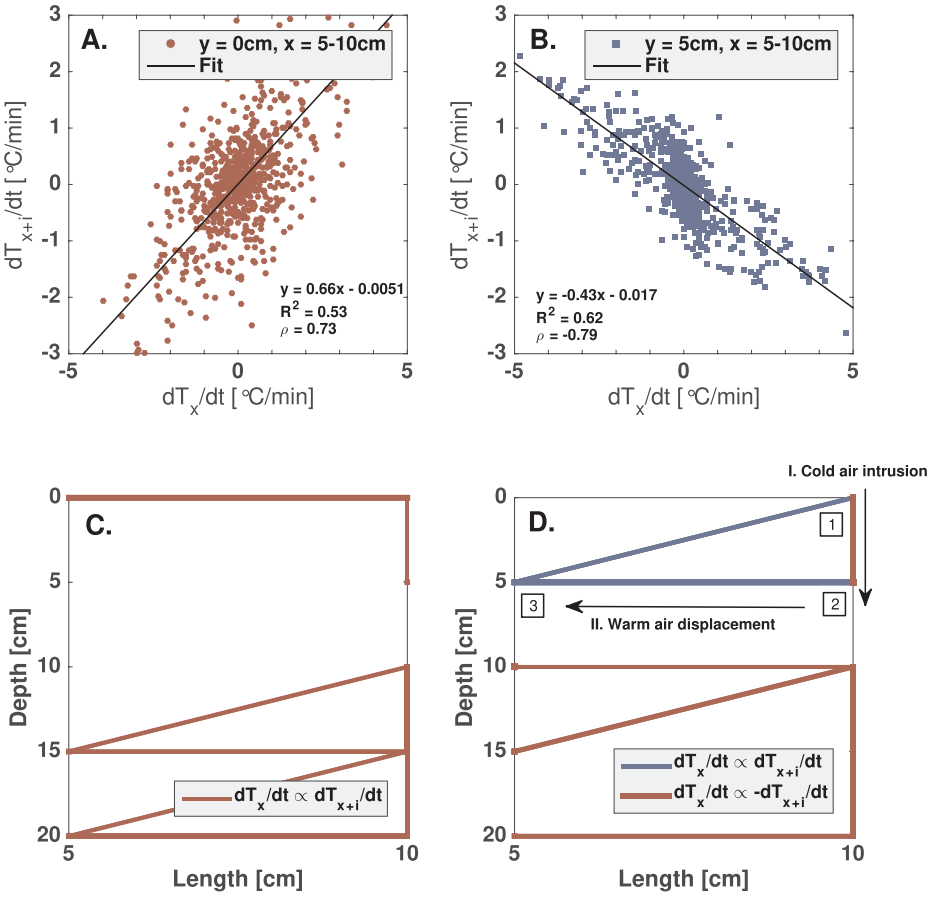

Fig. 8. Spatial correlation analysis of temperature fluctuations over time within the model soil fracture. (a) example of a strong positive correlation between fluctuations in temperature, observed at daytime between the 5 and 10 cm length position and 0 cm depth (i.e., horizontally along the surface). (b) example of a strong negative correlation between fluctuations in temperature, observed at nighttime between the 5 and 10 cm length position at 5 cm depth (i.e., horizontally within the fracture). Spatial maps of strong correlations ($\rho > 0.5$) within the fracture at (c) daytime and (d) nighttime. Fig. 8A corresponds with the top-most line observed in Fig. 8C, and Fig. 8B corresponds with the second top-most line observed in Fig. 8D.

cracks are likely to lower this minimum threshold – C and BC soils have shown a maximum cracking depth range of 0.01–0.08 m and 0.04–0.25 m, respectively, at a volumetric soil moisture range of 21–25% (DeCarlo and Caylor, 2019), with deeper depths likely observed under drier conditions, like the pre-wetting phase observed. Cracks act as preferential pathways for rapid water flow into the subsurface (Hoogmoed and Bouma, 1980; Romkens and Prasad, 2006), thereby bypassing absorption by the surface layer of the soil, and create saturation depths comparable, if not far deeper, than the ones observed in Thomas and Hoon (2010). Soil moisture measurements recorded in our experiments reflect those at the surface and may not reflect differences in soil moisture at depth.

4.2.2. Termite activity

The BT soils and their burrows exhibit different CO_2 characteristics, both in terms of magnitude and dynamics due to subsoil termite presence. The termite species present in our soils (*M. Odontermes*) create active subterranean colonies as deep as 2 m below the surface and characterized by the cultivation of fungus gardens. In virtually all soils, they create hollow chimneys several meters high, which is capable of inducing the Venturi effect due to differentials in wind velocity at the top and base of the chimney (Turner, 1994) – however, in our field sites, the chimneys are absent, with mounds less than half a meter tall (Pringle et al., 2010). This is most likely due to the shrink-swell process unique to vertisols, whose cracks will naturally introduce mechanical weaknesses in the large structure and result in its collapse. Additionally,

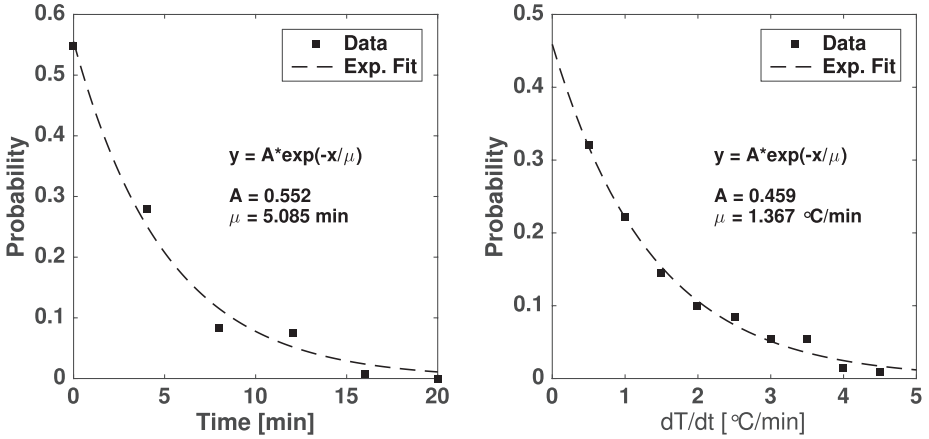

Fig. 9. Convection cell properties. (a) Distribution of time between convection cell events, with an exponential distribution fit shown. (b) Distribution of the magnitude of cold air intrusion within the fracture.

external winds can establish positive hydrostatic pressure gradients (Turner, 2001), but in African termite mounds, this has been shown to have no effect on CO_2 flux (Ocko et al., 2017), instead suggesting that free convection induced by thermal gradients in the soil profile is likely the primary mechanism for the observed elevated fluxes. These are likely further enhanced by increased subsoil temperature due to metabolic activity (Turner, 1994; Ganot et al., 2012).

We see evidence of convection in the BT burrows, particularly during the wetting phase, when CO_2 concentrations are elevated – CO_2 fluxes are lowest in the daytime (12 *h*00), increasing in the evening (18 *h*00) and peaking at night (22 *h*00), after which fluxes gradually decrease (6 *h*00). We also observe that daytime mean fluxes are lower than all mean night time fluxes. We note that the origin of the burrows created by the termite species is physically different from that of the fractures generated in the BC soils, and furthermore the particularities of vertisol morphology observed in the BC soils (e.g., soil layering effects) is unlikely to be present in these soils. However, functionally, these burrows play the same role in terms of soil-gas exchange, as they both mechanically enhance flux via thermal convection. Thus, we evaluate burrows in the context of fracture morphology, and furthermore evaluate both the BC and BT burrows soils as those with mechanical enhancements present. Theoretically, BT burrow morphology meets the minimum criteria for thermally-induced convection (Table 2), showing a fracture permeability k of 7.5×10^{-5} – 3.6×10^{-4} m^2 if we approximate it as a fracture (using the burrow diameter as a proxy for crack aperture), 2–3 orders of magnitude higher than those observed in the BC soils. Large morphological variability is observed, however, with depth and diameter ranging between 0.1 and 1.03 m and 1–28.6 cm, respectively. Furthermore, due to a combination of termite activity and shrink-swell, burrows were regularly created and/or sealed, and at times we were able to observe burrows within some of the BT soil sites, primarily during the drying phase. These two factors are likely to contribute to the wide range in flux observed.

CO_2 flux shows a nonlinearly positive relationship with soil moisture in the BT burrows, with fluxes during the wetting phase about an order of magnitude higher than those during the drying phase. Similar positive correlations were observed between CO_2 flux and soil moisture in termite mounds (Jamali et al., 2013), though not all termite species show this correlation. The relationship is less clear in the BT soils, which may be due to a combination of the hidden influence of BT burrows below the BT soil sites, which changes with time, and the negative correlation between decreasing soil moisture and increasing crack porosity and width, which increase the soil surface area available for diffusive fluxes. Several outlier BT fluxes that are comparable in magnitude to values observed in the BT burrows are present in the drying phase, which may further suggest that BT burrows contribute to BT flux, albeit at a lesser degree.

4.3. Integrating soil mechanics and soil carbon release

In the beginning of this study, we defined two primary controls in the context of CO_2 flux dynamics and distribution: soil crack mechanics, and soil carbon release. Limitations on either control can inhibit CO_2 flux magnitude and distribution in particular ways. Crack-induced enhancement occurs primarily by the extent of thermal convection, which is a function of crack depth due to the exposure of vertical thermal gradients in the soil. Larger crack apertures also simultaneously non-linearly increase CO_2 fluxes and are exponentially less frequent than smaller crack apertures, creating a long tail of outlier fluxes that can be orders of magnitude larger. Decreasing soil moisture increases both crack depth and aperture for a given soil and enhances flux, though outlier fluxes may still occur in undisturbed vertisols due to the sudden degassing of CO_2 from trapped crack air spaces in the soil layer. Soil carbon release enhancement shows positive tendencies to precipitation pulse and shifting between wetting/drying regimes, a tendency seen in most water-limited environments. CO_2 flux rates in carbon-limited soils experience large pulses following rainfall events and the re-wetting of the soil, the magnitude and fluctuation of which is positively correlated with the intensity of rainfall. Diurnal temperature fluctuations can affect soil carbon production and flux as well, with warmer environments generating higher microbial activity, though a sufficiently high soil moisture is required. Meanwhile, termite activity and their cultivation of fungi can provide consistently elevated levels of CO_2 in an otherwise organically poor soil environment. Fluxes in these carbon-enhanced soils are much higher in magnitude. Note that the effect that these controls have on CO_2 flux are not entirely independent from one another (e.g., precipitation pulses, particularly heavy ones, can enhance carbon flux pulse, but may also seal sections of the soil crack system due to shrink-swell).

The consequences of how these affect overall distribution of flux are shown in Fig. 10, where we plot the inverse cumulative probability distributions of the four soil classifications for each individual soil site. The results are mostly in agreement with our original conceptual framework. First evaluating the two extremes: in the mechanically-limited/carbon-limited soils, flux range and magnitude were low at each individual site, while in the mechanically-enhanced/carbon-enhanced soils, site flux range and magnitude were both high; both soil types had low site-to-site variability (though it should be noted fewer sites were measured for these soil treatments). When both of the limitations on soil crack mechanics and carbon release were removed, as was the case in the burrows of the BT soils, the carbon-rich soil air is consistently vented out of the soil system via convective processes. This extended the CO_2 flux magnitude to its maximal range, and reduced site-to-site variability; a wide range of flux is observed due to the periodic nature of the convection process. In the mechanically-enhanced/carbon-limited soils, we observe an intermediate flux range, magnitude, and site-to-site variability; although all sites exhibit a wide range of flux, which suggests a convection process, flux magnitudes are variable, with some (but not all) sites over an order of magnitude higher than the diffusion-dominant soils. In these cases, limitations on carbon release mean that crack enhancement cannot consistently provide high fluxes of CO_2 rich air. However, in the mechanically-limited/carbon-enhanced soils, half of the measured sites exhibit a diffusive flux signature and magnitude identical to that of the mechanically-limited/carbon-limited soils, whereas the other half exhibit a convective flux signature with a magnitude between that of the low- and high-carbon soils. We hypothesize that this may be due to the regular termite-induced structural changes occurring at depth. We qualitatively observed the regular cycling of old and new burrows within active termite mounds, with activity particularly increased following rainfall events; it is likely that similar activity is taking place at depth, where burrows may become topologically linked with the superficial crack network, inducing a muted convection response. Even if the burrows are not topologically connected with the crack network, the reduced distance between these two morphologies can reduce the effective diffusion length necessary for outflux into the atmosphere (Levintal et al., 2017), which may also result in a muted version of the high-carbon convection signature. That there was no effect of high carbon release on flux magnitude in these soil sites suggests that a majority of the carbon produced by the termites may be vented through their burrows, and the flux measured is what

Table 2
Statistics of all visible burrows at each of the BT sites analyzed. Measurements taken in August 2014. N is the number of burrows per BT site. R, d, and k are the mean radius, depth, and fracture permeability of the termite burrows, respectively.

BT site	N	R [cm]	d [cm]	k [m^2]
1	15	1.9	44.2	0.00012033
2	49	1.5	42.1	0.000075
3	21	1.8	39.2	0.000108

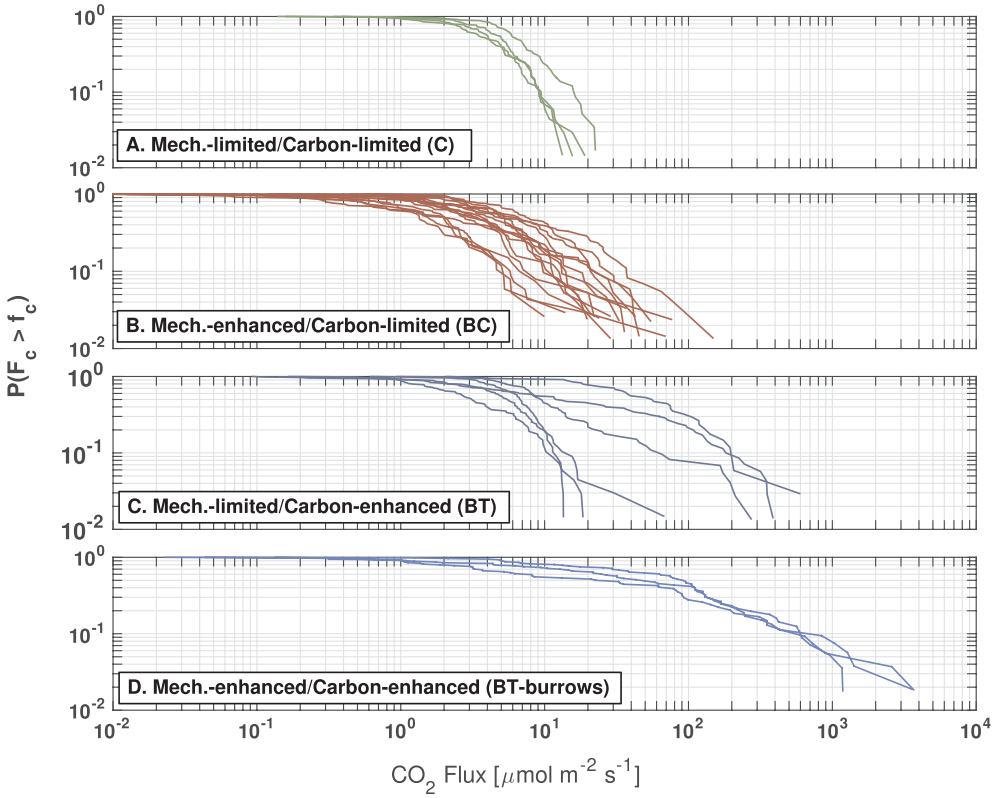

Fig. 10. Inverse cumulative probability distribution for (a) mechanically- limited/carbon-limited (C), (b) mechanically-enhanced/carbon-limited (BC), (c) mechanically-limited/carbon-enhanced (BT), and (d) mechanically- enhanced/carbon-enhanced (BT burrow) soils.

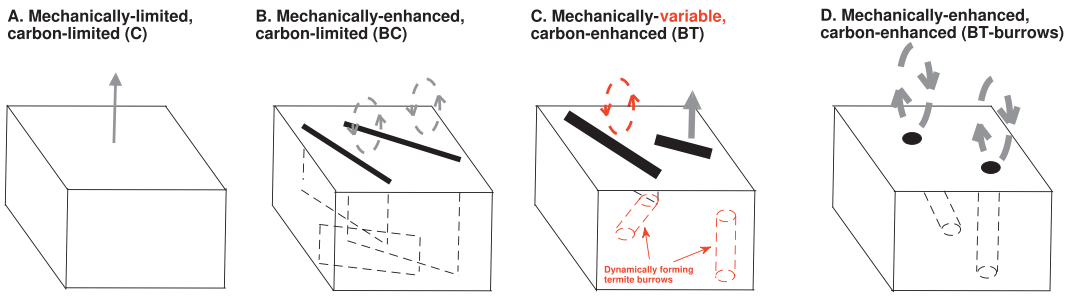

Fig. 11. Amended conceptual framework for the link between crack morphology and carbon flux in the four soil types classified in our cracked vertisols. Changes made from Fig. 1 are marked in red. (For interpretation of the references to color in this figure legend, the reader is referred to the web version of this article.)

the soil would have contributed regardless of termite presence. An amended conceptualization of the effect of these two controls on cracked vertisol flux is shown in Fig. 11 – as can be seen in Fig. 11C, if newly formed termite burrows are in close proximity to, or even connected with, the superficial crack network, the associated convective processes may dominate the otherwise diffusive flux signature of the BT crack network.

5. Conclusions

We show that crack morphology in faunally active vertisols enhances CO_2 flux by several orders of magnitude. This enhancement is primarily governed by crack depth and aperture, which enhances the onset of thermally-induced convection within the fracture. However, this enhancement is also modulated by the biotic dynamics present in dryland ecosystems, which is characterized by low soil carbon release. These fluxes show pulse behavior to precipitation and soil moisture increase, most likely due to the activation of soil heterotrophic communities. In certain sections of the soil, termite colonies can provide a persistently high source of soil CO_2 otherwise not present. The interaction of these two axes can produce distinct CO_2 flux distribution profiles: we see a large increase in flux range and magnitude when simultaneously shifting from a mechanically-limited/carbon-limited soil to a mechanically-enhanced/carbon-enhanced soil, with both exhibiting minimal site-to-site variability; while mechanically-enhanced/carbon-limited and mechanically-limited/carbon-enhanced soils exhibited intermediate flux signatures. Our results highlight how soil crack and macropore morphology can play a large role in the selective modulation and enhancement of CO_2 flux dynamics in dryland ecosystems.

Declaration of Competing Interest

The authors declare that they have no known competing financial interests or personal relationships that could have appeared to influence the work reported in this paper.

Acknowledgments

This research was carried out under Government of Kenya research clearance permit No. NCST/RCD/12B/012/42. We would like to thank John Gitonga, Boniface Kimathi, Moses Kioko, George Koech, and Peter Ekomwa for their invaluable assistance in the field. We also thank the Mpala Research Centre and its staff for their logistical support. The KLEE plots were built and maintained by grants from the James Smithson Fund of the Smithsonian Institution (to A.P. Smith), The National Geographic Society (Grants 4691-91 and 9106-12), the National Science Foundation (LTREB DEB 97-07477, 03-16402, 08-16453, 12-56004, and 12-56034) and the African Elephant Program of the U.S. Fish and Wildlife Service (98210-0-G563) (to T.P. Young, C. Riginos, and K.E. Veblen).

References

Adams, J.E., Hanks, R.J., 1964. Evaporation from soil shrinkage cracks. Soil Sci. Soc. Am. Proc. 28, 281–284.
Adams, J.E., Richie, J.T., Burnett, E., Fryrear, D.W., 1969. Evaporation from a simulated soil shrinkage crack. Soil Sci. Soc. Am. Proc. 33, 609–613.
Ahmad, N., Mermut, A., 1996. Vertisols and technologies for their management. Elsevier, Amsterdam.
Allaire, S.E., Lafond, J.A., Cabral, A.R., Lange, S.F., 2008. Measurement of gas diffusion through soils: comparison of laboratory methods. J. Environ. Modeling 10, 1326–1336.
Appel, T., 1998. Non-biomass soil organic N: the substrate for N mineralization flushes following soil drying-rewetting and for organic N rendered $CaCl_2$-extractable upon soil drying. Soil Biol. Biochem. 30, 1445–1456.
Baldocchi, D., Tang, J.W., Xu, L.K., 2006. How switches and langs in biophysical regulators affect spatial-temporal variation of soil respiration in an oak-grass savanna. J. Geophys. Res. Biogeosci. 111, G02008.
Batjes, N.H., 1996. Total C and N in soils of the world. Eur. J. Soil Sci. 47, 151–163.
Birch, H.F., 1958. The effect of soil drying on humus decomposition and nitrogen release. Plant Soil 10, 9–31.
Bonachela, J.A., Pringle, R.M., Sheffer, E., Coverdale, T.C., Guyton, J.A., Caylor, K.K., Tarnita, C.E., 2015. Termite mounds can increase the robustness of dryland ecosystems to climatic change. Science 347, 651–655.
Bond-Lamberty, B., Thomson, A., 2010. Temperature-associated increases in the global soil respiration record. Nature 464, 579–582.
Breecker, D.O., J Yoon, LA Michel, TM Dinka, SG Driese, JS Mintz, LC Nordt, KD Romanak, and CLS Morgan. 2013. CO2 concentrations in vertisols: seasonal variability and shrink-swell, In: SG Driese, LC Nordt, PJ McCarthy (Eds.). New Frontiers in Paleopedology and Terrestrial Paleoclimatology, SEPM special publication No. 104. Pp. 35-45.
Cox, P.M., Betts, R.A., Jones, C.D., Spall, S.A., Totterdell, I.J., 2000. Acceleration of global warming due to carbon-cycle feedbacks in a coupled climate model. Nature 408, 184–187.
Craine, J.M., Wedin, D.A., Chapin, F.S., 1999. Predominance of ecophysiological controls on CO2 flux in a Minnesota grassland. Plant Soil 207, 77–86.
Davidson, E.A., Belk, E., Boone, R.D., 1998. Soil water content and temperature as independent or confounded factors controlling soil respiration in a temperate mixed hardwood forest. Glob. Change Biol. 4, 217–227.
Davidson, E.A., Janssens, I.A., Luo, Y.Q., 2006. On the variability of respiration in terrestrial ecosystems: moving beyond Q10. Glob. Change Biol. 12, 154–164.
DeCarlo, K.F., Caylor, K.K., 2019. Biophysical effects on soil crack morphology in a faunally active dryland vertisol. Geoderma 334, 134–145.
Denef, K., Six, J., Bossuyt, H., Frey, S.D., Elliot, E.T., Merckx, R., Paustian, K., 2001. Influence of dry-wet cycles on the interrelationship between aggregate, particulate organic matter, and microbial community dynamics. Soil Biol. Biochem. 33, 1599–1611.
Eswaran, H., Van Den Berg, E., Reich, P., 1993. Organic carbon in soils of the world. Soil Sci. Soc. Am. J. 57, 192–194.
Etiope, G., 1999. Subsoil CO_2 and CH_4 and their advective transfer from faulted grassland to the atmosphere. J. Geophys. Res. 104, 16889–16894.
Fierer, N., Schimel, J.P., 2003. A proposed mechanism for the pulse in carbon dioxide production commonly observed following the rapid rewetting of a dry soil. Soil Sci. Soc. Am. J. 67, 798–805.
Flechard, C.R., Neftel, A., Jocher, M., Ammann, C., Leifeld, J., Fuhrer, J., 2007. Temporal changes in soil pore space CO_2 concentration and storage under permanent grassland. Agric. For. Meteorol. 142, 66–84.
Follett, R.F., 2001. Soil management concepts and carbon sequestration in cropland soils. Soil Tillage Res. 61, 77–92.
Ganot, Y., Dragila, M.I., Weisbrod, N., 2012. Impact of thermal convection on air circulation in a mammalian burrow under arid conditions. J. Arid Environ. 2012, 51–62.
Hogberg, P., Nordgren, A., Buchmann, N., Taylor, A.F.S., Ekblad, A., Hogberg, M.N., Nyberg, G., Ohoson-Lofvenius, M., Read, D.J., 2001. Large-scale forest girdling shows that current photosynthesis drives soil respiration. Nature 411, 789.
Hoogmoed, W.B., Bouma, J., 1980. A simulation model for predicting infiltration into cracked clay soil. Soil Sci. Soc. Am. J. 44, 458–461.
Houghton RA. 1995. Changes in the storage of terrestrial carbon since 1850. In: Lal R, JM Kimble, E Levine, and BA Stewart (Eds.), Soils and Global Change. CRC, Boca Raton, FL. Pp. 45-65.
Huxman, T.E., Snyder, K.A., Tissue, D., Leffler, A.J., Ogle, K., Pockman, W.T., Sandquist, D.R., Potts, D.L., Schwinning, S., 2004. Precipitation pulses and carbon fluxes in semiarid and arid ecosystems. Oecologia 141, 254–268.
Ikitoo, E.C., Okalebo, J.R., Othieno, C.O., 2011. Towards sustainable land use in vertisols in Kenya: Challenges and opportunities. In: Innovations as Key to the Green Revolution in Africa. Springer, Netherlands, pp. 661–675.
Jamali, H., Livesley, S.J., Hutley, L.B., Fest, B., Arndt, S.K., 2013. The relationships between termite mound CH_4/CO_2 emissions and internal concentration profiles are species specific. Biogeosciences 10, 2229–2240.
Kishne, A.S., Morgan, C.L.S., Miller, W.L., 2009. Vertisol crack extent associated with gilgai and soil moisture in the Texas Gulf Coast Prairie. Soil Sci. Soc. Am. J. 73, 1221–1230.
Kowalski AS, P Serrano-Ortiz, IA Janssens, S Sanchez-Moral, S Cuezva, F Domingo and L Alados-Arboledas. 2008. Can flux tower research neglect geochemical CO2 exchange? Agricultural Forest Meteorology 148:1045-1054.
Kuang, X., Jiao, J.J., Li, H., 2013. Review on airflow in unsaturated zones induced by natural forcings. Water Resour. Res. 49, 6137–6165.
Lapwood, E.R., 1948. Convection of a fluid in a porous medium. Proc. Cambridge Philos. Soc. 44, 508–521.
Levintal, E., Dragila, M.I., Kamai, T., Weisbrod, N., 2017. Free and forced gas convection in highly permeable, dry porous media. Agric. For. Meteorol. 232, 469–478.
Lewicki, J.L., Evans, W.C., Hilley, G.E., Sorey, M.L., Rogie, J.D., Brantley, S.L., 2003. Shallow soil CO_2 flow along the San Andreas and Calaveras Faults, California. J. Geophys. Res. Solid Earth 108 (B4), 2187.
Lewicki, J.L., Hilley, G.E., Tosha, T., Aoyagi, R., Yamamoto, K., Benson, S.M., 2007. Dynamic coupling of volcanic CO_2 flow and wind at the Horseshoe Lake tree kill, Mammoth Mountain, California. Geophys. Res. Lett. 34, L03401.
Liu, X., Wan, S., Su, B., Hui, D., Luo, Y., 2002. Response of soil CO_2 efflux to water manipulation in a tallgrass prairie ecosystem. Plant Soil 240, 213–223.
Loik, M.E., Breshears, D.D., Lauenroth, W.K., Belnap, J., 2004. A multi-scale perspective of water pulses in dryland ecosystems: Climatology and ecohydrology of the western USA. Oecologia 141, 269–281.
Luo, Y., Zhou, X., 2006. Soil respiration and the environment. Academic Press.
Massman, W.J., Sommerfeld, R.A., Mosier, A.R., Zeller, K.F., Hehn, T.J., Rochelle, S.G., 1997. A model investigation of turbulence-driven pressure-pumping effects on the rate of diffusion of CO_2, N_2O, and CH_4 through layered snowpacks. J. Geophys. Res. Atmospheres 102, 18851–18863.
Miller, W.L., Kishne, A.S., Morgan, C.L.S., 2010. Vertisol morphology, classification, and seasonal cracking patterns in the Texas Gulf Coast Prairie. Soil Survey Horizons 41, 10–16.
Moldrup, P., Olesen, T., Yoshikawa, S., Komatsu, T., Rolston, D.E., 2004. Three-porosity model for predicting the gas diffusion coefficient in undisturbed soil. Soil Sci. Soc. Am. J. 68, 750–759.
Nachshon, U., Weisbrod, N., Dragila, M.I., 2008. Quantifying air convection through surface-exposed fractures: A laboratory study. Vadose Zone J. 7, 948–956.
Nield, D.A., 1982. Onset of convection in a porous layer saturated by an ideal gas. Int. J. Heat Mass Transf. 25, 1605–1606.
Ocko, S.A., King, H., Andreen, D., Bardunias, P., Turner, J.S., Soar, R., Mahadevan, L., 2017. Solar-powered ventilation of African termite mounds. Journal of Exerimental Biology 220, 3260–3269.
Pringle, R.M., Doak, D.F., Brody, A.K., Jocque, R., Palmer, T.M., 2010. Spatial pattern enhanced ecosystem functioning in an African savanna. PLoS Biol. 8 (5), e1000377.
Raich, J.W., Potter, C.S., 1995. Global patterns of carbon-dioxide emissions from soils. Global Biogeochem. Cycles 9 (1), 23–26.
Raich, J.W., Potter, C.S., Bhagawati, D., 2002. Interannual variability in global soil respiration, 1980–94. Glob. Change Biol. 8, 800–812.
Reichstein, M., Tenhunen, J.D., Roupsard, O., Ourcival, J.M., Rambal, S., Dore, S., Valentini, R., 2002. Ecosystem respiration in two Mediterranean evergreen Holm Oak forests: Drought effects and decomposition dynamics. Funct. Ecol. 16, 27–39.
Rey, A., 2015. Mind the gap: non-biological processes contributing to soil CO_2 efflux. Glob. Change Biol. 21, 1752–1761.
Reynolds, J.F., Maestre, F.T., Kemp, P.R., Stafford-Smith, D.M., Lambin, E., 2007. Natural and human dimensions of land degradation in drylands: causes and consequences. In: Terrestrial Ecosystems in a Changing World. Springer, Berlin, Heidelberg, pp. 247–257.
Rochette, P., Ellert, B., Gregorich, E.G., Desjardins, R.L., Pattey, E., Lessard, R., Johnson, B.G., 1997. Description of a dynamic closed chamber for measuring soil respiration and its comparison with other techniques. Can. J. Soil Sci. 77, 195–203.
Romkens, M.J.M., Prasad, S.N., 2006. Rain infiltration into swelling/shrinking/cracking soils. Agric. Water Manag. 86, 196–205.
Sanchez-Canete, E.P., Serrano-Ortiz, P., Kowalski, A.S., Oyonarte, C., Domingo, F., 2011. Subterranean CO_2 ventilation and its role in the net ecosystem carbon balance of a karstic shrubland. Geophys. Res. Lett. 38, L09802.
Selim, H.M., Kirkham, D., 1970. Temperature and water content changes during drying as influenced by cracks: a laboratory experiment. Soil Sci. Soc. Am. Proc. 34, 565–569.
Schimel, D.S., 1995. Terrestrial ecosystems and the carbon cycle. Glob. Change Biol. 1, 77–91.
Schlesinger, W.H., 1995. Overview of the global carbon cycle. In: Kimble, J.M., Levine, E., Stewart, B.A. (Eds.), Lal R. Soils and Global Change. CRC, Boca Raton, FL, pp. 9–25.
Schlesinger, W.H., Andrews, J.A., 2000. Soil respiration and the global carbon cycle. Biogeochemistry 48, 7–20.
Serrano-Ortiz, M Roland, Sanchez-Moral, S., Janssens, I.A., Domingo, F., Godderis, Y., Kowalski, A.S., 2010. Hidden, abiotic CO_2 flows and gaseous reservoirs in the

terrestrial carbon cycle: Review and perspectives. Agric. For. Meteorol. 150, 321–329.
Sponseller, R.A., 2007. Precipitation pulses and soil CO_2 flux in a Sonoran Desert ecosystem. Glob. Change Biol. 13, 426–436.
Stewart, R.D., Abou Najm, M.R., Rupp, D.E., Lane, J.W., Uribe, H.C., Arumi, J.L., Selker, J.S., 2015. Hillslope run-off thresholds with shrink-swell clay soils. Hydrol. Process. 29, 557–571.
Tang, J.W., Baldocchi, D.D., 2005. Spatial-temporal variation in soil respiration in an oak-grass savanna ecosystem in California and its partitioning into autotrophic and heterotrophic components. Biogeochemistry 73, 183–207.
Tang, J.W., Baldocchi, D.D., Xu, L., 2005. Tree photosynthesis modulates soil respiration on a diurnal time scale. Glob. Change Biol. 11, 1298–1304.
Thomas, A.D., Hoon, S.R., Linton, P.E., 2008. Carbon dioxide fluxes from cyanobacteria crusted soils in the Kalahari. Appl. Soil Ecol. 39, 254–263.
Thomas, A.D., Hoon, S.R., 2010. Carbon dioxide fluxes from biologically-crusted Kalahari Sands after simulated wetting. J. Arid Environ. 74, 131–139.
Thomas, A.D., Hoon, S.R., Dougill, A.J., 2011. Soil respiration at five sites along the Kalahari Transect: Effects of temperature, precipitation pulses and biological soil crust cover. Geoderma 167–168, 284–294.
Turner, J.S., 1994. Ventilation and thermal constancy of a colony of a southern African Termite (Odontermes transvaalensis: Macrotermitinae). Journal of Arid Environments 28, 231–248.
Turner, J.S., 2001. On the mound of macrotermes michaelseni as an organ of respiratory gas exchange. Physiological and Biochemical Zoology: Ecological and Evolutionary Approaches 74, 798–822.
Virmani, S.M., Sahrawat, K.L., Burford, J.R., 1982. Physical and chemical properties of vertisols and their management. In: Twelfth International Congress of Soil Science. Indian Society of Soil Science, New Delhi, pp. 80–93.
Weeks EP. 1993. Does wind blow through Yucca Mountain, In: Proceedings of Workshop V: Flow and Transport through Unsaturated Fractured Rock Related to High-Level Radioactive Waste Disposal, DD Evans and TJ Nicholson (Eds.), U.S. Nuclear Regulatory Committee, NUREG CP-0040, pp. 45-53.
Weisbrod, N., Dragila, M.I., 2006. Potential impact of convective fracture venting on salt-crust build-up and ground-water salinization in arid environments. Journal of Arid Environments 65, 386–399.
Weisbrod, N., Dragila, M.I., Nachshon, U., Pillersdorf, M., 2009. Falling through the cracks : The role of fractures in Earth-atmosphere gas exchange. Geophys. Res. Lett. 36, L02401.
Xu, L., Baldocchi, D.D., Tang, J., 2004. How soil moisture, rain pulses and growth alter the response of ecosystem respiration to temperature. Global Biogeochem. Cycles 18, GB4002.
You, K., Zhan, H., 2013. Comparisons of diffusive and advective fluxes of gas phase volatile organic compounds (VOCs) in unsaturated zones under natural conditions. Adv. Water Resour. 52, 221–231.
Young, T.P., Okello, B.D., Kinyua, D., Palmer, T.M., 1997. KLEE: A long-term multi-species herbivore exclusion experiment in Laikipia, Kenya. African Journal of Range Forage Science 14, 94–102.